Fast and potent bactericidal membrane lytic activity of PaDBS1R1, a novel cationic antimicrobial peptide

Luz N Irazazabal, William F Porto, Isabel C.M. Fensterseifer, Eliane S.F. Alves, Carolina Matos, Antônio C.S. Menezes, Mário R Felício, Sónia Gonçalves, Nuno Santos, Suzana M Ribeiro, et al.

Fast and potent bactericidal membrane lytic activity of PaDBS1R1, a novel cationic antimicrobial peptide

Luz N. Irazazabal[a,b], William F. Porto[b,h,i], Isabel C.M. Fensterseifer[a,b], Eliane S.F. Alves[c,d], Carolina O. Matos[c], Antônio C.S. Menezes[d], Mário R. Felício[e], Sónia Gonçalves[e], Nuno C. Santos[e], Suzana M. Ribeiro[h,j], Vincent Humblot[f], Luciano M. Lião[c], Ali Ladram[g], Octavio L. Franco[b,h,*]

[a] Programa de Pós-graduação em Patologia Molecular, Universidade de Brasília, Brasília, DF 70910-900, Brazil
[b] Centro de Análises Proteômicas e Bioquímicas, Programa de Pós-graduação em Ciências Genômicas e Biotecnologia, Universidade Católica de Brasília, Brasília, DF, Brazil
[c] Instituto de Química, Universidade Federal de Goiás, Goiânia, GO 74690-900, Brazil
[d] Universidade Estadual de Goiás, Unucet, Anápolis, GO 75132-903, Brazil
[e] Instituto de Medicina Molecular, Faculdade de Medicina, Universidade de Lisboa, Av. Professor Egas Moniz, 1649-028 Lisboa, Portugal
[f] Sorbonne Université, CNRS, Laboratoire de Réactivité de Surface, LRS, F-75252 Paris, France
[g] Sorbonne Université, CNRS, Institut de Biologie Paris-Seine, IBPS, BIOSIPE, F-75252 Paris, France
[h] S-Inova Biotech, Pós-graduação em Biotecnologia, Universidade Católica Dom Bosco, Campo Grande, MS, Brazil
[i] Porto Reports, Brasília, DF, Brazil
[j] Programa de Pós-Graduação em Ciências da Saúde, Universidade Federal da Grande Dourados, Dourados, MS, Brazil

ARTICLE INFO

ABSTRACT

Antimicrobial peptides (AMPs) are promising candidates for the development of future antibiotics. In an attempt to increase the efficacy of therapeutic AMPs, computer-based design methods appear as a reliable strategy. In this study, we evaluated the antimicrobial efficiency and mechanism of action of a novel designed AMP named PaDBS1R1, previously designed by means of the Joker algorithm, using a fragment of the ribosomal protein L39E from the archaeon *Pyrobaculum aerophilum* as a template. PaDBS1R1 displayed low micromolar broad-spectrum antimicrobial activity against Gram-negative (MIC of 1.5 μM) and Gram-positive (MIC of 3 μM) bacteria, including carbapenem-resistant *Klebsiella pneumoniae* (MIC of 6.25 μM) and methicillin-resistant *Staphylococcus aureus* (MIC of 12.5 μM), without cytotoxicity towards HEK-293 cells. In addition, membrane permeabilization and depolarization assays, combined with time-kill studies and FEG-SEM imaging, indicated a fast membrane permeation and further leakage of intracellular content. Biophysical studies with lipid vesicles show a preference of PaDBS1R1 for Gram-negative bacteria-like membranes. We investigated the three-dimensional structure of PaDBS1R1 by CD and NMR analyses. Our results suggest that PaDBS1R1 adopts an amphipathic α-helix upon interacting with hydrophobic environments, after an initial electrostatic interaction with negative charges, suggesting a membrane lytic effect. This study reveals that PaDBS1R1 has potential application in antibiotic therapy.

1. Introduction

Given the increasing emergence of multidrug resistance in common pathogens, the development of effective new drugs has become a global health emergency. Consequently, there is a growing clinical need for novel types of antimicrobial agents to which the microorganisms have not been exposed. Furthermore, pharmaceutical companies have abandoned or cut back the production of new antimicrobial agents since only two novel classes of antibiotics have reached the market in the past two decades, including oxazolidinone (linezolid by Pfizer) and a cyclic lipopeptide (daptomycin by Cubist) [1]. In this context, the field of antimicrobial peptides (AMPs) research is increasingly gaining attention as a possible source of future antibiotics. To date, thousands of AMP sequences have now been experimentally validated [2]. AMPs

are short (< 50 amino acid residues) amphipathic molecules typically containing about 50% hydrophobic residues, and most of them exhibit positive charge [3]. Their cationic/amphipathic character allows them to interact with various types of lipid membranes.

AMPs have been described to rapidly kill or slow down the growth of pathogens, including multidrug resistant bacteria, as well as to be involved in the activation and modulation of adaptive immunity mechanisms [4,5]. In contrast to conventional antibiotics, which target specific proteins, AMPs interact with microbial membranes through electrostatic and non-specific interactions [6]. The exact AMP mechanism of action is a matter of controversy. However, there is a widespread acceptance that the main mode of action involves perturbation and/or permeabilization of the cell membranes [7]. All the proposed mechanisms (ion channel/pore formation and/or detergent-like effect) emphasize the molecular basis of their attraction to membranes [4,8]. In addition, AMPs exhibit multiple modes of action, including membrane disruption enhancing membrane permeability and/or disturbing key cellular processes by interacting with intracellular targets [7–9].

Biological membranes are complex systems containing a large variety of proteins and lipids arranged as amphipathic bilayers. A widely accepted notion is that electrostatic interactions between the positively charged residues of AMPs and the negatively charged phospholipid head groups of the target pathogen cell membrane are involved in the first step of interaction of the peptides (binding and accumulation) with the membrane, while the amphipathic character of AMPs enables membrane perturbation [10,11]. Hence, as a requirement for the non-mediated interactions, AMPs exhibit a conformational transition. Most AMPs lack a secondary structure in aqueous environments but adopt an amphipathic α-helical structure upon interacting with membranes [11–13].

Although there is evidence of multiple cases of pathogen acquired resistance to AMPs [14–16], their versatile character allows the rational design of novel sequences, inspired by natural peptides, where modifications of one single amino acid residue could lead to a more effective peptide. The improvement of AMP activity and applications in clinical therapy can be addressed by rationally designed sequences [17].

The interactions between α-helical AMPs and bacterial membranes are guided by several physicochemical parameters and involve the following rules: increasing the hydrophobicity leads to an increase in affinity to lipids; increasing the hydrophobic moment favours the peptide folding into α-helix; and last, increasing the net charge leads to a more favourable interaction with anionic membranes [18]. However, the linguistic model [19] considers the AMPs as a formal language with a grammar composed of several rules, the patterns. Based on this model, Porto et al. [20] developed the Joker algorithm that generates antimicrobial peptides by means of insertion of an antimicrobial pattern in peptide sequences, turning them into AMPs.

Herein, the antimicrobial efficiency of PaDBS1R1 (PKILNKILGKIL-RLAAAFK) was investigated. This peptide was previously obtained by rational design, engineering a fragment of the ribosomal protein L39E from the hyperthermophilic archaeon *Pyrobaculum aerophilum*, using the Joker algorithm [20]. The potent broad-spectrum antimicrobial activity and no cytotoxicity against human embryonic cells were demonstrated. Furthermore, the ability of PaDBS1R1 to induce membrane permeabilization/depolarization and to kill bacteria was evaluated. The peptide effects on bacterial cells were visualized by FEG-SEM imaging. Finally, to understand the interaction of PaDBS1R1 with the target membrane, a functional and structural analysis was performed using lipid vesicles, CD experiments and NMR spectroscopy.

2. Materials and methods

2.1. Synthesis and mass spectrometry analysis

The peptides PaDBS1R1 (PKILNKILGKILRLAAAFK, MW 2107.6 Da) and PaDBS1R1-amide (PKILNKILGKILRLAAAFK-NH2, MW 2106.6 Da) were synthesized *via* Fmoc chemistry using the Liberty Blue™ automated microwave peptide synthesizer (CEM Corporation), a PAL-NovaSyn TG resin (Merck Millipore), and a systematic double-coupling protocol. Cleavage and deprotection of the peptidyl resin were achieved by incubation of the resin with an acidic cocktail (95% TFA, 2.5% triisopropylsilane, 2.5% water) for 3 h at room temperature. Resin was removed by filtration and the crude peptide was precipitated with cold diethyl ether ($3000 \times g$, 15 min, 4 °C), washed with the same solvent, and dried under a stream of nitrogen. Purification was performed by reversed-phase HPLC on a semi-preparative Nucleosil C-18 column (5 μm, 250 mm × 10 mm, Interchim SA). The homogeneity and identity of the synthetic peptide were assessed by MALDI-TOF MS analysis using the Applied Biosystems 4700 proteomics analyser (see Supplementary Fig. S1). Melittin was kindly provided by Dr. Christophe Piesse (Peptide Synthesis Platform, IBPS, FR 3631, Sorbonne Université, Paris, France). All peptides were obtained with 98% of purity.

2.2. Minimum inhibitory concentration (MIC) determination

The Gram-negative bacteria *Escherichia coli* (ATCC 25922), *Pseudomonas aeruginosa* (ATCC 27853), *Acinetobacter baumannii* (ATCC 19606), *Klebsiella pneumoniae* (ATCC 13883), and a clinical isolate of carbapenem-resistant *K. pneumoniae* (3259271), the Gram-positive bacteria *Staphylococcus aureus* (ATCC 25923), a clinical isolate of methicillin-resistant *S. aureus* (7133623), and *Enterococcus faecalis* (ATCC 29212) were cultured in Lysogeny Broth (LB). The two Gram-positive species, *Streptococcus pyogenes* (ATCC 19615) and *Listeria ivanovii* (Li 4pVS2) were cultured in Brain Heart Infusion (BHI) broth, whereas the fungi *Candida albicans* (ATCC 90028) and *C. parapsilosis* (ATCC 22019) were cultured in Yeast Peptone Dextrose medium (YPD). As previously described [21], MIC was determined in 96-well microtitration plates by growing microorganisms in the presence of 2-fold serial dilution of PaDBS1R1. Briefly, logarithmic phase culture of bacteria were centrifuged and suspended in MH (Muller Hinton) broth to an A_{630} of 0.01 (10^6 cfu·ml^{-1}), except for *S. pyogenes*, *L. ivanovii*, *E. faecalis* and *Candida* species, which were suspended in their respective growth medium. Microtiter plate wells were used with aliquots of 50 μl each of the diluted culture followed by the addition of 50 μl of the diluted peptide (200 to 1 μM, final concentrations). The antimicrobial susceptibility was monitored after overnight incubation at 37 °C (30 °C for fungi) by measuring the change in A_{630} value using a microplate reader. MIC was expressed as the lowest peptide concentration that completely inhibited the growth of the microorganism, corresponding to the average value from three independent experiments, each performed in triplicate with positive (0.7% formaldehyde) and negative (without peptide) inhibition controls [22].

2.3. Cytotoxic properties

The cytotoxicity of PaDBS1R1 was assessed on the human leukemia monocyte cell line THP-1 after their differentiation into macrophages by adding phorbol 12-myristate 13-acetate (PMA) in RPMI medium, and also on the human embryonic kidney cell line HEK-293, cultured in DEMEM medium. The cell viability was quantified after peptide incubation using a methylthiazolyldiphenyl-tetrazolium bromide (MTT)-based microassay [23]. Briefly, cells were seeded on 96-well culture plates at a density of 5×10^5 cells·ml^{-1} and incubated 72 h at 37 °C with 100 μl of PaDBS1R1 (12.5 to 200 μM, final concentrations). After adding 10 μl of MTT (5 mg·ml^{-1}) to each well and incubating for 4 h in the dark, formazan crystals were dissolved, incubated 1 h at 37 °C under shaking (150 rpm), and the absorbance was measured at 570 nm. The half maximal inhibitory concentration (IC_{50}), which corresponds to the peptide concentration producing 50% cell death, was determined with GraphPad Prism 5.0 software. Results were expressed as the mean of three independent experiments performed in triplicate.

2.4. In vitro selectivity index calculation

According to Porto et al. [24], the *in vitro* selectivity index of PaDBS1R1 was calculated using the following equation:

$$TI = \frac{\sqrt[n]{\prod_{i=1}^{n} Cytotoxic_i}}{\sqrt[m]{\prod_{j=1}^{m} Antibacterial_j}} \tag{1}$$

where n is the number of cytotoxicity assays and m is the number of antimicrobial assays with different bacteria. For values higher than the maximum concentration tested, 2-fold the maximum tested value was assumed (*e.g.* if the value is > 100, it was considered as 200) [25].

2.5. Preparation of large unilamellar vesicles (LUVs)

Large unilamellar vesicles with ~100 nm of diameter (LUVs) were obtained by extrusion of multilamellar vesicles (MLVs), as described elsewhere [26]. 1-palmitoyl-2-oleoyl-*sn*-glycero-3-phosphocoline (POPC), 1-Palmitoyl-2-oleoyl-*sn*-glycero-3-phospho-(1′-*sn*-glycerol) (POPG), 1-palmitoyl-2-oleoyl-*sn*-glycero-3-phosphoethanolamine (POPE) and cardiolipin (CL) were obtained from Avanti Polar Lipids (Alabaster, AL, USA), while cholesterol (Chol) was obtained from Sigma (St. Louis, MO, USA). The LUVs studied were zwitterionic (pure POPC and POPC:Chol 70:30) or anionic (POPC:POPG 70:30, POPC:POPG:CL 65:30:05 and 25:70:05, and POPE:POPG:CL 65:30:05 and 25:70:05), with the latter four lipid compositions mimicking the membranes of Gram-negative and -positive bacteria, respectively. Stock solutions of MLVs of various lipid compositions were kept at 4 °C overnight before measurements, and extruded on the day of the measurement. 4-(2-Hydroxyethyl)-1-piperazineethanesulfonic acid (HEPES) buffer, 150 mM NaCl, pH 7.4, was used in these preparations and measurements.

2.6. Laurdan lipid packing assay

Lipid vesicles were labelled by incubation with the fluorescent dye 6-dodecanoyl-2-dimethylaminonaphtalene (Laurdan) to a final probe/lipid ratio of 1:300 (3 mM of lipid and 9.90 μM concentration), in order to increase the sensitivity without disturbing the membrane properties. Laurdan can give insights into the changes in the lipid packing after interaction with the peptide, due to the ability of the probe to sense changes in the polarity of the environment [27,28]. The mixture was incubated in the dark for 30 min at 25 °C. The changes were followed by fluorescence spectroscopy using a Varian Cary Eclipse fluorescence spectrophotometer (Mulgrave, Australia). Laurdan emission spectra in the absence and presence of different concentrations of peptide (from 0.5 to 9.0 μM of PaDBS1R1) were measured after 1 h of incubation, between 400 and 600 nm, using 350 nm as excitation wavelength and 4 and 10 nm for excitation and emission bandwidths, respectively. To quantify the spectral changes, Laurdan generalized polarization (G_p) was calculated as follows [29]:

$$G_p = \frac{I_{440} - I_{490}}{I_{440} + I_{490}} \tag{2}$$

where I_{440} and I_{490} are the emission intensities at 440 nm and 490 nm (corresponding to the gel and liquid crystalline lipid phases), respectively. Assays were done in triplicate, with the error bars representing the standard deviation.

2.7. Membrane dipole potential assay

After extrusion, LUVs were diluted in HEPES buffer with a final concentration of 500 μM, and incubated overnight at 25 °C with 10 μM di-8-ANEPPS, for maximum dye incorporation, with gentle agitation and protected from light. This probe assesses the differences induced by the peptide on the membrane dipole potential. For the measurements,

the final lipid concentration was 200 μM with 1 μM of the dye present. The suspensions were incubated with the peptide (0.5 to 9.0 μM) for 1 h. Excitation spectra and the ratio of intensities at the excitation wavelengths of 455 and 525 nm ($R = I_{455}/I_{525}$) were obtained with the emission set at 670 nm to avoid membrane fluidity-related artefacts [30–32]. Excitation and emission slits for these measurements were set to 5 and 10 nm, respectively. The variation of R with the peptide concentrations was analysed by a single binding site model [33]:

$$\frac{R}{R_0} = 1 + \frac{R_{min}/R_0 \cdot [Peptide]}{K_d + [Peptide]} \tag{3}$$

with the R value normalized for R_0, the value in the absence of peptide. R_{min} defines the asymptotic minimum value of R, and K_d is the dissociation constant. The fitting of this equation to the experimental data was done by non-linear regression using GraphPad Prism 6. Error bars represent the standard deviation of triplicates.

2.8. Dynamic light scattering and zeta-potential

Dynamic light scattering experiments were carried out on a Malvern Zetasizer Nano ZS (Malvern, UK) with a backscattering detection at 173°, equipped with a He-Ne laser (λ = 632.8 nm), at 25 °C, using disposable polystyrene cells, as described elsewhere [34]. Briefly, LUV suspensions were diluted in HEPES buffer and then filtered using a syringe filter with 0.45 μm pore size (Whatman, Florham Park, NJ, USA). Lipid concentration was kept constant at 200 μM, and the peptide concentration varied in the same range as the methods described above. Samples were left equilibrating for 15 min at 25 °C. Normalized intensity autocorrelation functions were analysed using the CONTIN method [35,36], yielding a distribution of diffusion coefficients (D). The measured D was used for the calculation of the hydrodynamic diameter (D_H) through the Stokes-Einstein relationship [34]. Sets of 15 measurements (with 10 runs each) for the liposomes in the absence and presence of the different concentrations of peptide were done. The zeta-potential (ξ) of the liposomes was determined at 25 °C from the mean of 15 measurements (100 runs each), in the absence and presence of different PaDBS1R1 concentrations, using DST 1060 disposable zeta cells (Malvern, UK) with gold electrodes, after 15 min of equilibration time [37]. Values of viscosity and refractive index were set at 0.8872 cP and 1.330, respectively [38]. Lipid concentration was the same as in the dynamic light scattering assays, in order to acquire high enough count rates. All data were processed using the Malvern DTS software, after three independent experiments.

2.9. SYTOX green uptake assay

The PaDBS1R1-induced permeation of the cytoplasmic membrane of *S. aureus* ATCC 25923 and *E. coli* ATCC 25922 was measured using the SYTOX Green (SG) uptake assay [39]. As previously described [21], exponentially growing bacteria (6×10^5 cfu·ml^{-1}) were suspended in PBS after centrifugation (1000 ×g, 10 min, 4 °C) and three washing steps. 792 μl of the bacterial suspension were preincubated with 8 μl of 100 μM SG for 30 min at 37 °C in the dark. After peptide addition (200 μl, final concentration 6.25 μM), the fluorescence was measured for 1 h at 37 °C, with excitation and emission wavelengths of 485 and 520 nm, respectively. Three independent experiments were performed, and the results presented correspond to a representative experiment, including negative (PBS) and positive (melittin) controls.

2.10. Membrane depolarization

The cytoplasmic membrane depolarization activity of PaDBS1R1 was measured using *S. aureus* ATCC 25923 and *E. coli* ATCC 25922 and the membrane potential sensitive probe 3,3′-dipropylthiadicarbocyanine iodide (DiSC3(5)) [40]. As previously described [21],

exponentially growing bacteria were centrifuged, washed with PBS and re-suspended to an A_{630} of 0.1 (1×10^7 cells·ml^{-1}) in the same buffer. 700 μl of bacteria were pre-incubated with 1 μM DiSC3(5) in the dark for 10 min at 37 °C, and then 100 μl of 1 mM KCl were added in order to equilibrate the cytoplasmic and external K$^+$ concentrations. After addition of peptide (6.25 μM), the fluorescence was monitored at 37 °C for 20 min with excitation and emission wavelengths of 622 and 670 nm, respectively. Three independent experiments were performed and the results presented correspond to a representative experiment, including negative (PBS) and positive (melittin) controls.

2.11. Time-kill studies

As previously described [41], exponentially growing bacteria in LB (*S. aureus* ATCC 25923 and *E. coli* ATCC 25922) were harvested by centrifugation, washed and suspended in PBS (10^6 cfu·ml^{-1}, final concentration). After incubation of 100 μl of this bacterial suspension with PaDBS1R1 (2-fold and 4-fold above the MIC for *S. aureus* and *E. coli*, respectively), aliquots of 10 μl were withdrawn at different times, diluted and spread onto LB agar plates. After overnight incubation at 37 °C, CFU were counted. Two experiments were carried out in triplicates. Controls were run without peptide.

2.12. FEG-SEM imaging

Scanning Electron Microscopy with Field Emission Gun (FEG-SEM) was used to obtain high-resolution images of the effect of PaDBS1R1 on the Gram-positive bacteria *L. ivanovii* (Li 4pVS2) and the Gram-negative bacteria *P. aeruginosa* (ATCC 27853). Bacteria in mid-logarithmic phase were collected by centrifugation, washed twice with PBS, and suspended in the same buffer (2×10^7 cfu·ml^{-1}). 200 μl of the bacterial suspension were incubated 1 h at 37 °C with PaDBS1R1 (6.25 μM). Negative controls were run in buffer without peptide. Cells were fixed with 2.5% glutaraldehyde. FEG-SEM images were recorded with a Hitachi SU-70 Field Emission Gun Scanning Electron Microscope. The samples (20 μl of inoculum deposited and dried under dry nitrogen on gold plates) were fixed on an alumina SEM support with a carbon adhesive tape and were observed without metal coating. Secondary electron detector (SE-Lower) was used to characterize the samples. The accelerating voltage was 1 kV and the working distance was around 15 mm. At least five to ten different locations were analysed on each surface, leading to a minimum of 100 single cells observed.

2.13. Circular dichroism spectroscopy

Circular dichroism (CD) assays were carried out using a JASCO J-815 spectropolarimeter equipped with a Peltier temperature controller (model PTC-423 L/15). Measurements were recorded at 25 °C and performed in quartz cells of 1 mm path length, between 190 and 260 nm, at 0.2 nm intervals. Six or eight repeat scans at a scan-rate of 50 nm·min^{-1}, 1 s response time and 1 nm bandwidth were averaged for each sample and for the baseline of the corresponding peptide-free sample. Concentrations of 50 μM of PaDBS1R1 at 25 °C in 20 mM DPC and 20 mM SDS at pH 4 (2 mM Na-acetate buffer), pH 7 (2 mM Tris-HCl buffer) and pH 10 (2 mM glycine-NaOH buffer) were used. POPC:POPG (3:1, mol/mol) phospholipid vesicles at 500 μM were also used. After subtracting the baseline from the sample spectra, CD data were processed with the Spectra Analysis software, which is part of Spectra Manager Platform. The relative helix content (H) according to the number of peptide bonds (n) was calculated by the formula $[\theta]_{222}^{obs} = (f_H - ik/n).[\theta]_\infty$ [42].

2.14. NMR experiments

NMR experiments were carried out on a Bruker Avance III 500 spectrometer operating at 11.75 T. One-dimensional spectra of ^{1}H were acquired. In addition, we conducted the two-dimensional experiments: Total correlation spectroscopy (^{1}H-^{1}H TOCSY) experiment was recorded with 120 transients of 4096 data points, 256 t1 increments. Nuclear Overhauser effect spectroscopy (^{1}H-^{1}H NOESY) experiments were recorded with 48 transients of 4096 data points, 512 t1 increments and mixing time of 250 ms. Heteronuclear single-quantum correlation (^{1}H-^{13}C) experiment, edited mode, was acquired with 176 transients of 4096 points for each free induction decay and 256 t1 increments. SO-FAST heteronuclear multiple-quantum coherence (^{1}H-^{15}N sf-HMQC) experiment was recorded with 1024 data points and 80 t1 increments and 8936 transients. NMR samples were prepared in H$_2$O:D$_2$O (9:1, v/v); the PaDBS1R1 concentration was 1 mM in the presence of 100 mmol·l^{-1} of SDS-d$_{25}$, and 5% (m/v) of 4,4-dimethyl-4-silapentane-1-sulfonic acid (DSS) was added as a chemical shift reference. The experiments were performed in 30 mM phosphate buffer at pH 7.0 and 25 °C. Assignment of the backbone and side-chain ^{1}H cross peaks was achieved following the sequential assignment methodology developed by Wüthrich [43]. Restraint distances used in structural calculations were obtained from 2D NOESY. Two-dimensional experiments were processed using the nmrPIPE [44] and nmrVIEW [45] software. Structural calculations were performed with XPLOR-NIH program [46,47]. The NMR structures and restraint files were submitted to PDB, with the code 2N9R (http://www.rcsb.org/pdb/explore/explore.do?structureId=2N9R).

3. Results

3.1. Antimicrobial activity evaluation

The effect of PaDBS1R1 was evaluated against several bacterial strains and *Candida* species. As shown in Table 1, PaDBS1R1 displays a potent broad-spectrum antibacterial activity against Gram-positive and -negative bacteria at low micromolar concentrations with MICs in the range of 1.5–3 μM, except against *Enterococcus faecalis* for which PaDBS1R1 was poorly active (MIC = 50 μM). Additionally, we tested the effect of PaDBS1R1-amide against the Gram-negative bacteria

Table 1
Antimicrobial activity and cytotoxicity of PaDBS1R1 and PaDBS1R1-amide.

Microorganism	MIC (μM)	
	PaDBS1R1	PaDBS1R1-amide
Gram-negative bacteria		
Escherichia coli ATCC 25922	1.5	1.5
Pseudomonas aeruginosa ATCC 27853	1.5	1.5
Klebsiella pneumoniae ATCC 13883	1.5	ND[a]
Acinetobacter baumannii ATCC 19606	1.5	ND
Carbapenem-resistant *K. pneumoniae* (3259271)	ND	6.25
Gram-positive bacteria		
Staphylococcus aureus ATCC 25923	3	3
Streptococcus pyogenes ATCC 19615	3	ND
Listeria ivanovii	3	ND
Enterococcus faecalis ATCC 29212	50	ND
Methicillin-resistant *S. aureus* (7133623)	ND	12.5
Yeasts/fungi		
Candida albicans ATCC 90028	≥50	ND
C. parapsilosis ATCC 22019	25	ND

Human cells	IC$_{50}$ (μM)	
	PaDBS1R1	PaDBS1R1-amide
THP-1-derived macrophages	7.3 ± 3.0	ND
HEK-293	143.2 ± 30.9	ND

[a] Not determined. Minimum inhibitory concentration (MIC) and half maximal inhibitory concentration (IC$_{50}$) are expressed as average values from three independent experiments performed in triplicate.

Escherichia coli and *P. aeruginosa*, and also against the Gram-positive bacteria *Staphylococcus aureus*. For these strains, MIC values were identical to those obtained for the C-terminally non-amidated form (Table 1). Furthermore, we tested the activity of PaDBS1R1-amide against antibiotic-resistant bacteria (Gram-positive and negative). We observed a high activity against carbapenem-resistant *Klebsiella pneumoniae* (MIC = 6.25 μM) and against methicillin-resistant *S. aureus* (MIC = 12.5 μM) (Table 1). Also, PaDBS1R1 exhibits activity against the yeast *Candida parapsilosis* (MIC = 25 μM), whereas it was much less active against *C. albicans* (MIC $\geq$ 50 μM) (Table 1).

3.2. Time-kill kinetics

The killing effect of PaDBS1R1 (6.25 μM) was investigated against *E. coli* (ATCC 25922) and *S. aureus* (ATCC 25923). The peptide caused a rapid and complete killing of *E. coli* in < 5 min. For *S. aureus*, a slower killing kinetics was observed, with complete eradication of bacteria at 30 min. These results indicate that the potent effect of PaDBS1R1 against *E. coli* and *S. aureus* is bactericidal (Supplementary Fig. S2).

3.3. Cytotoxic properties towards human cells

We extended our study by investigating the cytotoxicity of PaDBS1R1 towards human cells, such as macrophages derived from the THP-1 human leukemia monocytic cell line, and also human embryonic kidney (HEK-293) cells, since the liver plays a key role in the systemic clearance of administered drugs. Our results indicate that PaDBS1R1 is not cytotoxic against HEK-293 cells, as indicated by the IC_{50} value (143.2 ± 30.9 μM) that was far above MIC values determined for the bacterial strains tested (1.5–12.5 μM) (Table 1). By contrast, the peptide shows cytotoxicity towards human THP-1-derived macrophages, as revealed by the much lower IC_{50} value (7.3 ± 3.0 μM) (Table 1). Together with the MIC data, we calculated the *in vitro* selectivity index of PaDBS1R1, reaching a value of 6.1. This value takes only into account the data from PaDBS1R1 non-amidated form (Table 1) and indicates a reasonable selectivity window, where a 6-fold administration would be necessary to reach a toxic effect. Being the *in vitro* selectivity index analogous to the therapeutic index, according to the U.S. Food and Drug Administration, a therapeutic index is considered narrow when it is below two, while for a safer drug, the higher the index, the better is the drug [48]. Therefore, PaDBS1R1 can be considered as a safe peptide.

3.4. PaDBS1R1-induced permeabilization of the bacterial cytoplasmic membrane

To study the ability of PaDBS1R1 to interact with the membrane of Gram-negative and Gram-positive bacteria, we evaluated the membrane permeability of a Gram-negative (*E. coli* ATCC 25922) and a Gram-positive reference strain (*S. aureus* ATCC 25923) after treatment with the peptide (6.25 μM). We monitored the permeability of the bacterial cytoplasmic membrane with the SYTOX Green (SG) uptake assay, using the membrane lytic peptide melittin (5 μM) as positive control. This known pore-forming AMP of 26 residues induces complete permeabilization and depolarization of both Gram-positive and Gram-negative bacterial membranes [49]. Fig. 1 reveals that PaDBS1R1 was able to permeate the bacterial membrane of *E. coli* (Fig. 1A) and *S. aureus* (Fig. 1B), as indicated by the increase of the fluorescence signal of the SG dye compared to the negative control (PBS). For *E. coli*, we observed a similar pattern of permeabilization with PaDBS1R1 and melittin. However, for *S. aureus*, the SG fluorescence signal was higher for PaDBS1R1 compared to melittin.

3.5. Bacterial cytoplasmic membrane depolarization induced by PaDBS1R1

The membrane-potential-sensitive probe DiSC3(5) was used to analyse the PaDBS1R1-induced depolarization of the bacterial
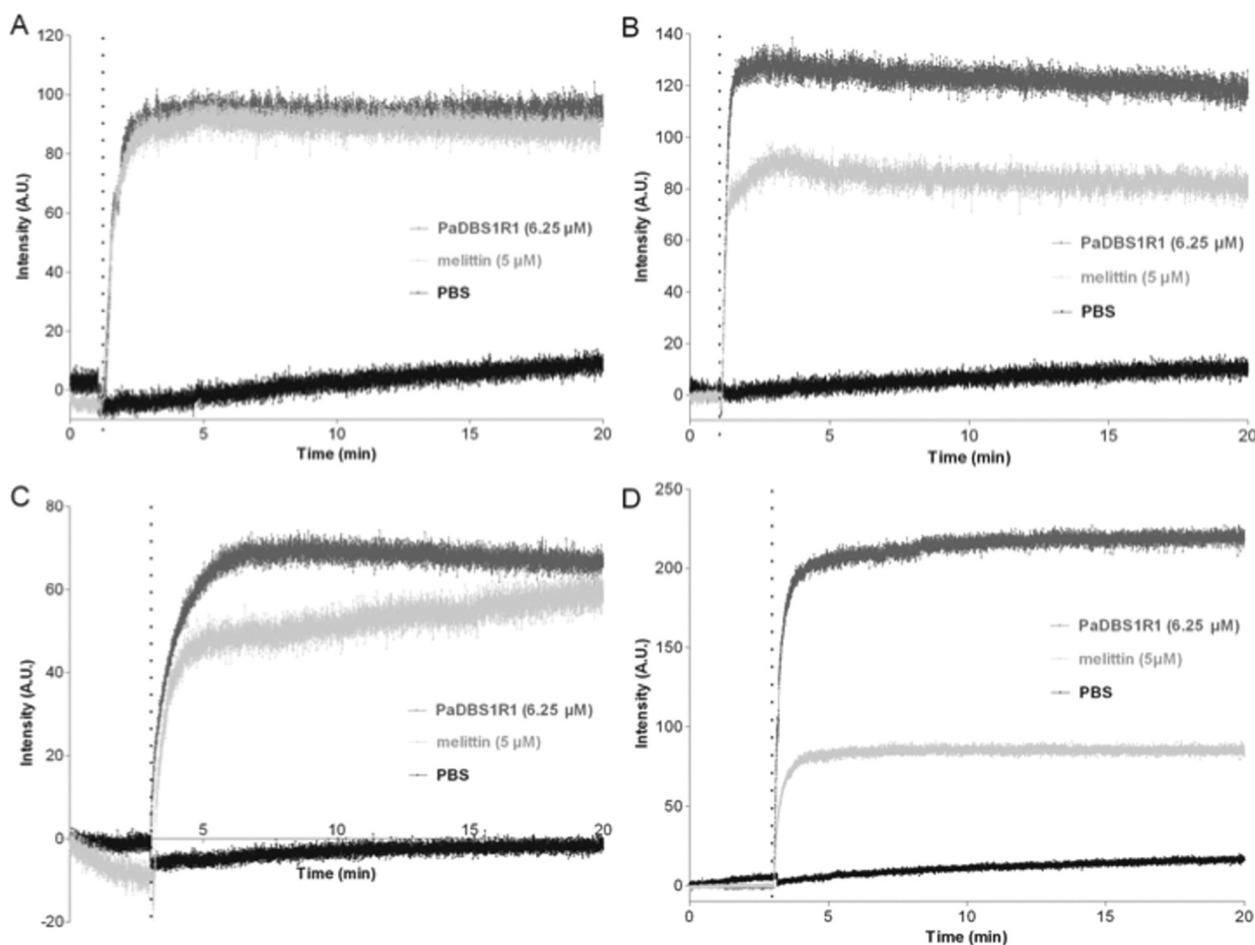
cytoplasmic membrane of *E. coli* and *S. aureus*. As shown in Fig. 1C and D, after incubation with the positive control melittin (5 μM), the membrane potential is lost and DiSC3(5) is released into the medium, triggering the increase of fluorescence. In the presence of PaDBS1R1 (6.25 μM), a complete depolarization of both *E. coli* (Fig. 1C) and *S. aureus* (Fig. 1D) membranes is rapidly achieved (< 5 min). The dissipation of the Gram-positive membrane potential occurred with a higher maximal threshold compared to the positive control. This is in line with the higher permeabilization observed.

3.6. Molecular mechanism of PaDBS1R1 interaction with membranes

In order to understand if the peptide interacts with membranes and changes their properties, studies using Laurdan, a dye that senses disturbances in the polarity of the environment [27], were carried out with membrane vesicles (Fig. 2A). The studies were done for different lipid compositions, including zwitterionic (POPC and POPC:Chol 70:30) and anionic membranes, with the intention of mimicking Gram-negative (POPC:POPG 70:30, POPC:POPG:CL 65:30:05 and POPE:POPG:CL 65:30:05) and Gram-positive (POPC:POPG:CL 25:70:05 and POPE:POPG:CL 25:70:05) bacterial membranes. Results are presented as generalized polarization (G_p) values calculated for each peptide concentration tested. Note that the different values obtained initially in the absence of peptide, for the different lipid compositions, are expected as a result of different polarity. Even so, it is possible to see that for POPC:POPG 70:30 and POPC:POPG:CL 65:30:05, the G_p values were similar (Fig. 2A), which allows us to infer that cardiolipin does not induce significant changes in the polarity of the membrane. An increase on the G_p initial value was observed for the lipid vesicles containing POPE, instead of POPC. Regarding the peptide effect, with the increase on PaDBS1R1 concentration only POPE:POPG:CL 65:30:05 vesicles had higher G_p values. For the others lipid vesicles tested, PaDBS1R1 did not induce changes in polarity nor in lipid packing.

Furthermore, we used the fluorescence probe di-8-ANEPPS to study changes in membrane dipole potential when the peptide adsorbs or interacts with the membrane. The excitation spectra of the dye allow us to confirm the perturbation induced by the peptide, depending on how the potential varies. Blue shifts in the excitation spectra denote an increase of the potential, whereas red shifts indicate a decrease. To assess these shifts, we calculated the ratio (R) of the fluorescence intensities measured with excitation at 455 and 525 nm, which gave us an insight about how the ratio changes with the increase in peptide concentration [30,50]. Fig. 2B represents the results obtained for each lipid composition, with the anionic vesicles with POPC on their composition showing a decrease in dipole potential (decrease in R), comparing with small changes or none in zwitterionic vesicles. Moreover, it is possible to observe that membranes mimicking Gram-negative bacteria have a greater interaction with the peptide compared with the others tested, corroborating the results obtained for the antimicrobial tests. From the data plotted, it is possible to apply an equation (Eq. (3), materials and methods) to fit the data, which allows us to calculate the apparent dissociation constant (K_D^{app}) and the asymptotic value of the normalized R_{min} for each lipid composition (Table 2) [31]. Again, the values obtained are in agreement with the curves, meaning that PaDBS1R1 has a greater affinity for negatively charged lipid vesicles containing POPC, expressed by the lowest K_D^{app} values obtained more accurately. Regarding both vesicles that contain POPE as the zwitterionic phospholipid, interestingly, they do not change their signal with the increase in PaDBS1R1 concentration, contrasting with their POPC homologous vesicles. This will be addressed below.

With the objective of studying the differences induced by PaDBS1R1 in the hydrodynamic diameter (D_H) of different lipid vesicles, dynamic light scattering (DLS) and zeta-potential measurements were conducted (Fig. 2C and D, respectively) [34]. DLS, indicates that the titration of the peptide only induced an aggregation profile in POPE:POPG:CL 65:30:05 Gram-negative bacteria-mimicking vesicles, presenting a high

Fig. 1. Effect of PaDBS1R1 on plasma membrane integrity of *E. coli* (ATCC 25922) and *S. aureus* (ATCC 25923). (A-B) Cytoplasmic membrane permeabilization of *E. coli* (A) and *S. aureus* (B) analysed by SYTOX Green (SG) uptake after addition (vertical dotted line) of PaDBS1R1 at a concentration of 6.25 μM. (C-D) Effect of PaDBS1R1 (6.25 μM) on the cytoplasmic membrane depolarization of *E. coli* (C) and *S. aureus* (D) observed with DiSC3(5). The membrane lytic peptide melittin (5 μM) was used as a positive control. The negative control PBS corresponds to the bacteria incubated with fluorescent probes without peptide. (For interpretation of the references to colour in this figure legend, the reader is referred to the web version of this article.)

D_H value in larger concentrations (342 ± 62 nm). POPE:POPG:CL 25:70:05 also lead to higher D_H values (152 ± 1.9 nm). All the other types of vesicle did not show size differences after peptide incubation.

By zeta-potential studies, changes induced by the peptide after electrostatic interaction with lipid vesicles can be tracked. The zeta-potential (ξ) is calculated through the electrophoretic mobility of the particles of the sample, in the presence of an electric field [51]. For PaDBS1R1, with the increase in concentration, the electrostatic interactions tend to be stronger, which is seen in the increase of the zeta-potential variation (Δξ, calculated as the difference between the values in the presence and absence of the peptide). Even so, the results are different considering the lipid composition, with the larger changes being seen in Gram-negative bacteria-mimicking vesicles (POPC:POPG 70:30, POPC:POPG:CL 65:30:05 and POPE:POPG:CL 65:30:05). Surprisingly, the changes induced in pure POPC vesicles were also extensive, which may be due to peptide accumulation at the membrane interface. The other zwitterionic vesicles (POPC:Chol 70:30) and the Gram-positive mimicking vesicles (POPC:POPG:CL and POPE:POPG:CL 25:70:05) showed small differences with the increase of peptide concentration.

3.7. Visualization of the antibacterial effect of PaDBS1R1 by FEG-SEM imaging

To clarify the detailed mechanisms of cell death at lethal AMP

concentrations, we used high-resolution scanning electron microscopy (FEG-SEM) to observe alterations in bacterial membrane integrity caused by PaDBS1R1. FEG-SEM analysis was performed on *P. aeruginosa* (ATCC 27853) and *Listeria ivanovii* (Li 4pVS2). Fig. 3 clearly shows that all bacterial cells were damaged after exposure to PaDBS1R1. We observed membrane deformation/blebbing for *P. aeruginosa* after contact with 3 μM or 50 μM of PaDBS1R1 (Fig. 3B–C), compared to untreated cells (Fig. 3A). In the case of *L. ivanovii*, the high activity of PaDBS1R1 was confirmed by the observation of numerous lysed cells and cell debris at 3 μM and 6.25 μM (Fig. 3E–F) in comparison to the control (Fig. 3D). Altogether, our results indicate potent bactericidal activity of PaDBS1R1 *via* a membranolytic mechanism.

3.8. Structural analyses of PaDBS1R1

The CD experiments demonstrate that, in aqueous solution at different pH values (pH 4, 7 and 10), the peptide assumes a random coil conformation, as shown in the spectra by a characteristic minimum at 198 nm (Supplementary Fig. S3A). In the presence of dodecylphosphocholine micelles (DPC), there is a more defined helical secondary structure of the peptide at neutral (Fig. 4B) and basic pH (data not shown) conditions. A greater structuring of PaDBS1R1 is observed in anionic micelles of sodium dodecyl sulphate (SDS) than DPC and POPC:POPG (Fig. 4A and B). In environments with SDS and neutral pH (Fig. 4A), the peptide adopts greater structuring, with an α-helical
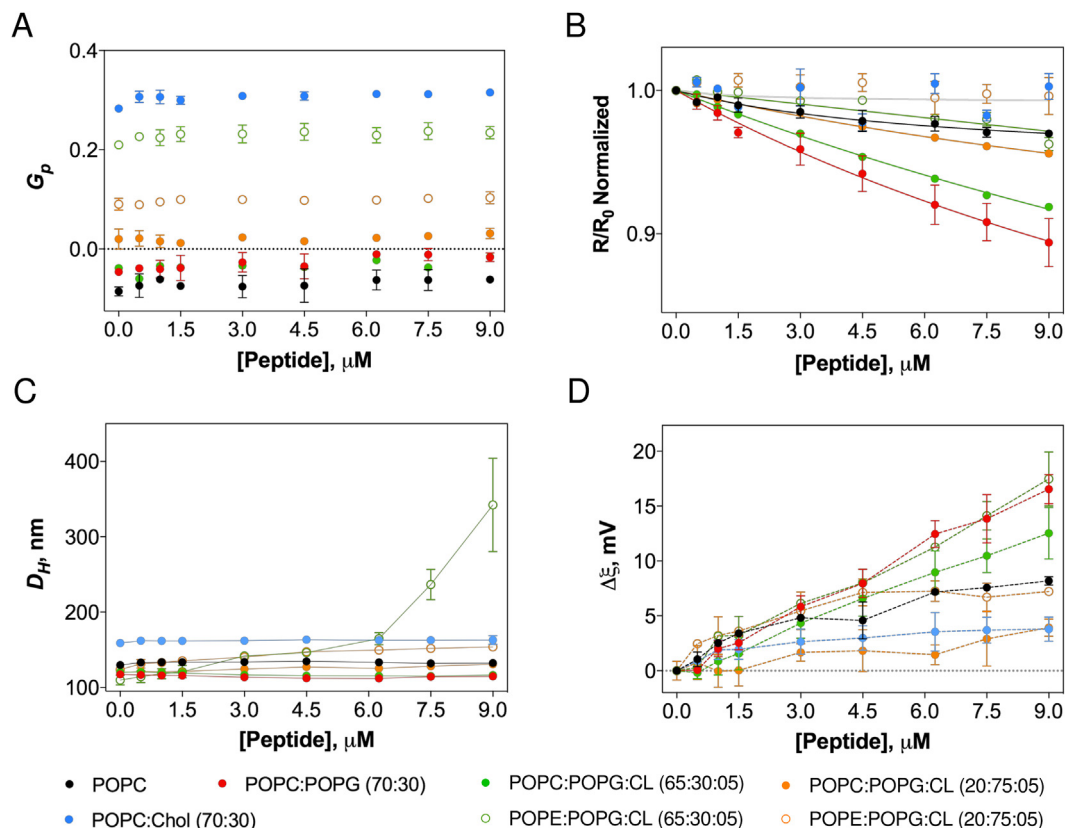
Fig. 2. Effects of PaDSB1R1 interactions with lipid vesicles. (A) Membrane lipid packing, (B) membrane dipolar potential, (C) hydrodynamic diameter and (D) zeta-potential variations in lipid vesicles, with the increasing of PaDBS1R1 concentration. Lipid vesicles at a final concentration of 3 mM (A) or 200 μM (B–D). (A) Laurdan at a final concentration of 9.90 μM, with excitation wavelength of 350 nm. Values of generalized polarization were calculated according to Eq. (2). (B) Di-8-ANEPPS at 1 μM, with excitation wavelengths of 455 and 525 nm, and with emission wavelength of 670 nm. Ratio ($R = I_{455}/I_{525}$) was calculated and normalized for the initial value. Fitting lines were adjusted with Eq. (3). Affinity parameters calculated are indicated in Table 2. The values obtained were the result of 15 measurements, with 10 runs (C) and 100 runs (D) each. Error bars represent the standard deviation of three independent measurements.

conformation, as evidenced by characteristic minimum at 208 and 222 nm and maximum at 190 nm. Similar behaviours are observed for PaDBS1R1 in the presence of anionic POPC:POPG (3:1) vesicles (Fig. 4B).

Therefore, the NMR analysis conditions were chosen considering the CD experiments (SDS media at pH 7). In order to study the three-dimensional structure of the peptide in micellar SDS, the proton assignments of PaDBS1R1 were obtained from the analysis of the TOCSY spectrum (Fig. 4C), showing residual intra-relations of each amino acid residue that comprises the peptide sequence. NOESY experiments also showed intra- and inter-residue correlations between amino acid residues that were spatially near (Fig. 4D). Using Wüthrich's method, the amino acid spin system and connectivity were assigned based on simultaneous analysis of TOCSY and NOESY [52]. Inter-proton distance restraints were derived from a NOESY spectrum (Fig. 4D). The NOE

connectivity (data not shown) showed the likely structure of PaDBS1R1. In this diagram it is not possible to confirm the correlations i, i + 3 concerning correlations 19HN-16Hα, 17HN-14Hα, 16HN-13Hα and 15HN-12Hα, due to the possible overlap of sequential and medium-range NOEs with similar shifts. Secondary structure prediction was performed according to the method proposed by Wishart et al. for peptides [53], using the nmrVIEW program interface. The chemical shift index (CSI) of Hα, Cα and N observed (Supplementary Fig. S3B) showed an α-helix between Lys2 and Lys19, based on the chemical shifts (experimental data). The chemical shifts of ^{13}C and ^{15}N were obtained through the experiments of HSQC and HMQC, respectively. These data were used in the TALOS+ method to predict peptide backbone phi (φ) and psy (ψ) torsion angles [54], indicating a valid prediction of NMR structure (data not shown). Moreover, it indicates α-helical conformation from Leu4 to Phe18.

Table 2

Values of apparent dissociation constants (K_D^{app}) and asymptotic value of the normalized minimum intensity ratio (R_{min}) calculated for lipid vesicles mimicking different cell membranes. Eq. (2) was used for the fitting of the data.

| Lipid composition	Mimicked membrane	Charge	K_D^{app} (μM)	R_{min}
POPC	Control	Zwitterionic	6.91 ± 2.62	−0.05 ± 0.01
POPC:Chol 70:30	Mammalian cells	Zwitterionic	n.a.[a]	n.a.[a]
POPC:POPG 70:30	Gram-negative bacteria	Negative	24.05 ± 7.16	−0.39 ± 0.09
POPC:POPG:CL 65:30:05	Gram-negative bacteria	Negative	38.22 ± 11.37	−0.43 ± 0.11
POPE:POPG:CL 65:30:05	Gram-negative bacteria	Negative	n.a.[a]	n.a.[a]
POPC:POPG:CL 25:70:05	Gram-positive bacteria	Negative	24.14 ± 14.40	−0.16 ± 0.08
POPE:POPG:CL 25:70:05	Gram-positive bacteria	Negative	n.a.[a]	n.a.[a]

[a] n.a. – not possible to apply the fit.
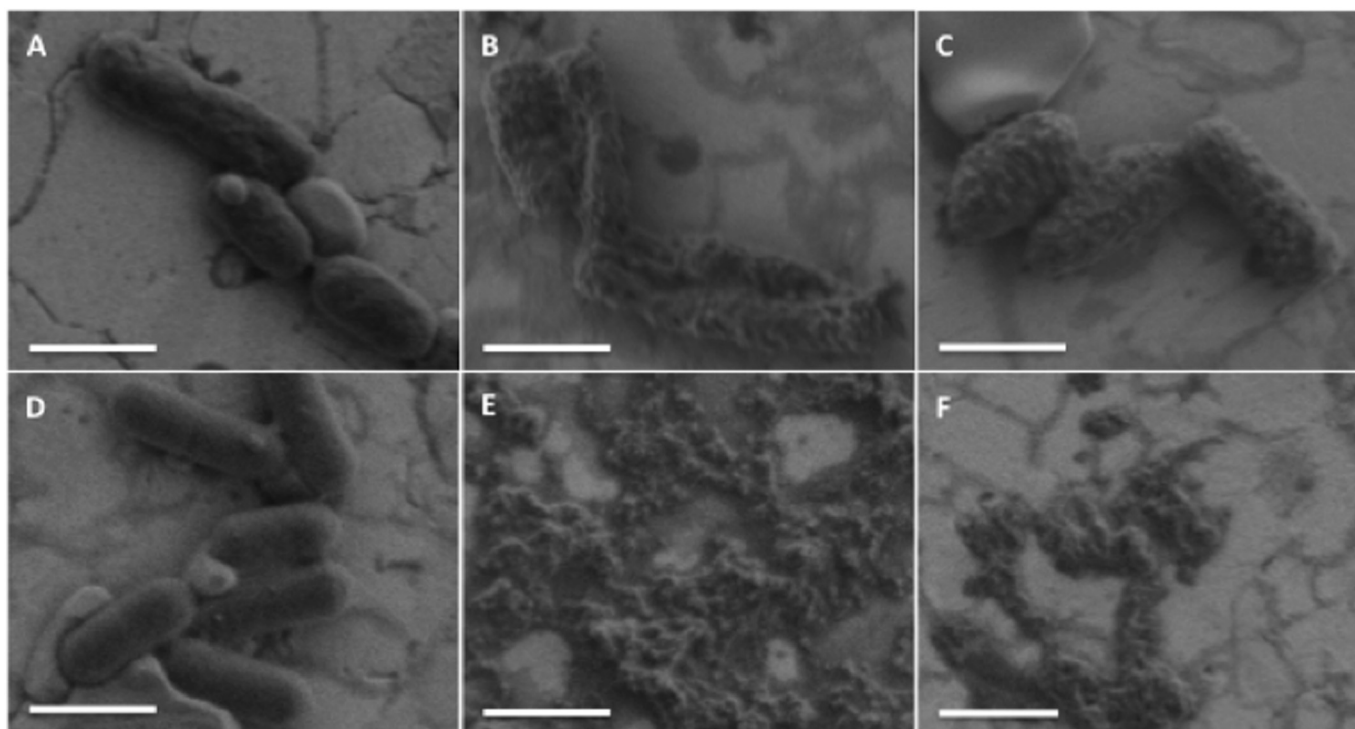
Fig. 3. FEG-SEM visualization of the effect of PaDBS1R1 on *P. aeruginosa* (A–C) and L. *ivanovii* (D–F). (A, D) Control without peptide. (B, C) *P. aeruginosa* after 1 h incubation with 3 μM and 50 μM of PaDBS1R1, respectively. (E, F) *L. ivanovii* treated 1 h with 3 μM and 6.25 μM of PaDBS1R1, respectively. Scale bar = 1 μM.

Predicted secondary structure elements of the CSI agreed with TALOS+ program method. After examining TALOS+, we continued our analysis using the method named quantitative evaluation of experimental NMR restraints (QUEEN) [55]. This method gives data that allow us to verify and validate the reliability of the restraints used through the low unique information content (I_{uni}). In addition, the average information content (I_{ave}) provides a measure of the overall importance of a restraint within the complete dataset, showing a primary significance for distance restraints (Supplementary Fig. S3C).

Intra-residual restrictions exhibited little structural information,
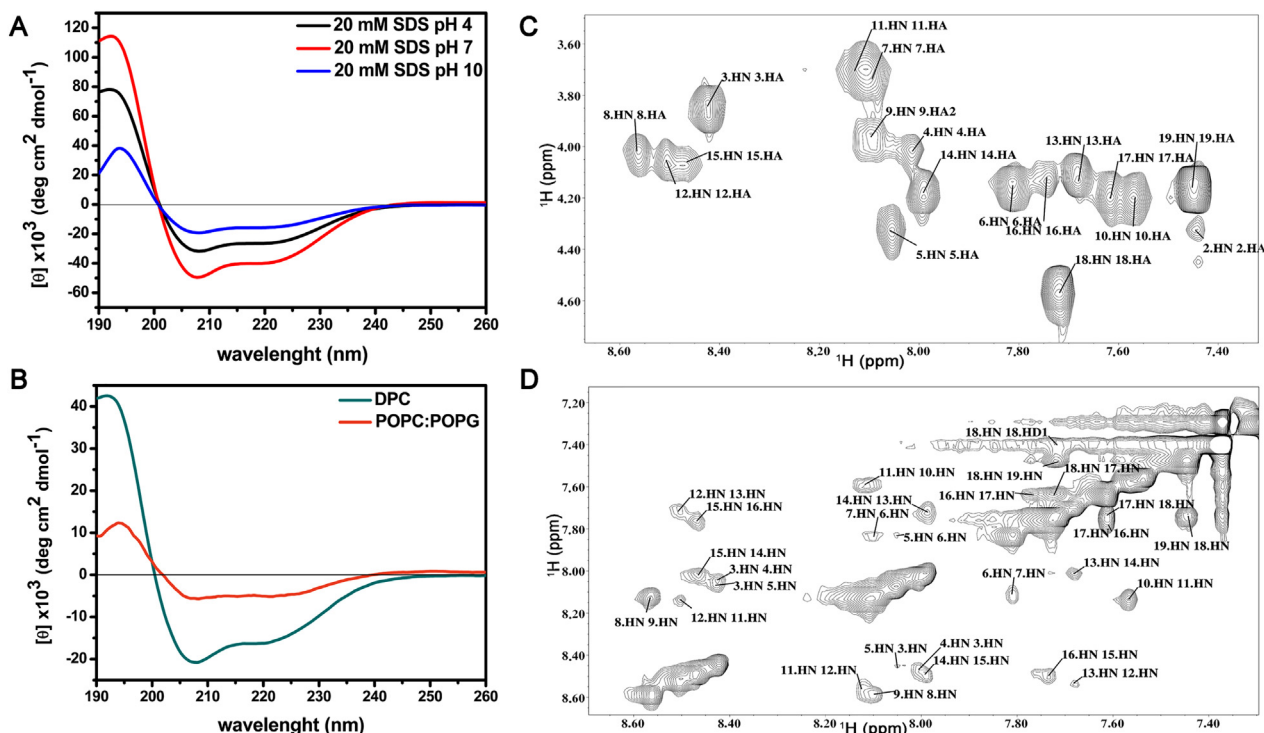
Fig. 4. Circular dichroism (CD) and NMR two-dimensional experiments ^{1}H-^{1}H-TOCSY and ^{1}H-^{1}H NOESY of PaDBS1R1. CD spectra performed with a concentration of 50 μM of PaDBS1R1 at 25 °C in (A) 20 mM SDS, pH 4, 7 and 10 (B) 20 mM DPC and 500 μM POPC:POPG (3:1), pH 7. (C) Fingerprint region of ^{1}H TOCSY contour map and (D) region of ^{1}H$_N$-^{1}H$_N$ NOESY contour map obtained for 1 mM of PaDBS1R1 in the presence of 100 mM of SDS-d$_{25}$.

Table 3
Structural statistics of the best 10 NMR structures of PaDBS1R1.

NOE RESTRAINTS	
Total number of distance restraints	278
Number of intra-residue restraints	175
Number of sequential restraints $(i, i + 1)$	84
Number of medium-range restraints $(i, i + j)_{j = 2,3,4}$	18
Number of long-range restraints $(|i\text{-}j| > 5)$	0
Dihedral angles	34
Hydrogen Bonds	0
RMSD (Å)[a] – All residues	
Backbone	0.77 ± 0.26
Backbone and heavy atoms	1.46 ± 0.37
RMSD (Å)[a,b] – Helical segment	
Backbone	0.52 ± 0.18
Backbone and heavy atoms	1.15 ± 0.30
Ramachandran plot analysis[c]	
Residues in most favoured regions	95.9%
Residues in additional allowed regions	4.1%
Residues in generously allowed regions	0.0%
Residues in disallowed regions	0.0%

[a] Data from MOLMOL using 10 lowest energy structures.
[b] From [4–18].
[c] Data from http://mordred.bioc.cam.ac.uk/~rapper/rampage.php.

although constituting a major part of data is important to confirm assignment and indicate the integrity of the datasets. We performed structure calculations using 278 distance restrictions, totalizing an average of 16.4 restrictions per residue. A total of 200 structures were calculated and the 20 lowest energy structures were selected for water refinement [56], from which the 10 lowest energy conformations represented a family of structures (Table 3).

The accuracy of the structures calculated by NMR was expressed as a function of the root-mean-square deviation (RMSD) [57]. The geometrical quality of the obtained models was an important validation of the structure obtained by NMR. Using the MOLMOL program [58], the set of 10 structures with the lowest energy scores was aligned. Table 3 presents statistics showing the precision and stereochemical quality of the peptide structures. The RMSD values highlight that the structures exhibit a good geometry with a good conformational flexibility, reflecting the internal dynamics of the molecule and the uncertainty deriving from the experimental data and computational conversion of the processes [59]. The existence of converging conformations shows the consistency and compatibility of the restrictions used in structural calculations.

The obtained structures were evaluated for their stereochemistry quality using the RAMPAGE Server (http://mordred.bioc.cam.ac.uk/~rapper/rampage.php), which gives the Ramachandran Plot [60,61] (data not shown). The combination of dihedral angles φ and ψ, based on steric considerations, indicated a good structural quality of 95.5% for the φ and ψ angles located in the α-helix region. Fig. 5C shows the overlap of the 10 lowest energy structures, highlighting in blue the polar amino acid residues. The amphipathic characteristics can be better observed in Fig. 5A (N-terminal (left) and C-terminal (right)), where the hydrophobic and hydrophilic residues are located on different faces. NMR spectroscopy showed that the peptide presented a well-defined α-helix covering residues between Leu4 and Phe18, when interacting with SDS micelles (model membrane).

All secondary structures of PaDBS1R1 obtained were consistent with the CSI prediction data, NOE panel and analysis of the TALOS+ and CD measurements. This result was confirmed by NMR experiments showing the position of each amino acid residue. The peptide was structured as a helix, as expected by the predictions of the CSI and TALOS+.

4. Discussion

In this study, we investigated the antibacterial activity of a 19-residue antimicrobial peptide (PKILNKILGKILRLAAAFK), named PaDBS1R1, designed from a non-antimicrobial sequence using the Joker algorithm [20]. Antimicrobial assays revealed that the new designed peptide displays high activity against a broad spectrum of microorganisms. We showed herein that PaDBS1R1 is not only active against Gram-negative and -positive bacteria, but is also highly potent with MICs in the low micromolar range (1.5–3 μM) (Table 1). It is known that several AMPs display post-translational modifications that can alter their biological activity, and that particularly C-terminally amidated peptides are often more effective than the non-amidated forms [62,63]. This could be due to the neutralization of the negatively charged C-terminal carboxylate, thus increasing the net positive charge of the peptide, and/or to the protection of the peptide from carboxypeptidase degradation. Thus, we decided to also investigate the antibacterial activity of carboxyamidated PaDBS1R1. When we compared the MIC values of PaDBS1R1-amide to those of the non-amidated form, we found no difference against the bacteria tested (E. coli, P. aeruginosa and S. aureus; see Table 1), suggesting that no increase of net positive charge and/or protection against carboxypeptidases are needed to enhance the potency of PaDBS1R1. In addition, PaDBS1R1-amide exhibited a potent activity against carbapenem-resistant K. pneumoniae (MIC = 6.25 μM) and methicillin-resistant S. aureus (MIC = 12.5 μM). It is thus likely that the acquired mechanisms of resistance in those bacterial clinical isolates do not affect PaDBS1R1 mode of action [64]. Further research on peptide selectivity provides encouraging data, as PaDBS1R1 exhibited no cytotoxic activity towards HEK-293 cells at MIC concentration. These findings support an optimistic outlook for potential therapeutic applications [65].

Several studies determined that the biological activity of most AMPs is based on permeabilization of microbial membranes [64,66]. The data in this work suggest the ability of PaDBS1R1 to induce permeabilization and depolarization of the cytoplasmic bacterial membrane (Fig. 1), likely leading to leakage of the intracellular content (Fig. 3), and finally cell death. The killing kinetics of PaDBS1R1 against bacteria indicated a faster complete killing for the Gram-negative E. coli (< 5 min), compared to the Gram-positive S. aureus (30 min), contributing to its therapeutic potential. As a matter of fact, there are examples of antimicrobial peptides presenting a short time of action against bacteria, starting their action in the first minutes in contact with cells, leading to a total death in about 15 min [67]. The time-kill outcome is consistent with the membrane permeabilization and depolarization experiments that show immediate effects of PaDBS1R1 on the integrity of the microbial membranes.

In order to study the biophysical changes that the peptide can induce in different types of biomembranes, studies using lipid vesicles were also assessed. It is well documented that the use of membrane mimicking models can give insights into the interactions of membrane-active peptides with different targets [68]. The methodologies that can be applied in this kind of study are also already documented, with the use of Laurdan and di-8-ANEPPS dyes in fluorescence spectroscopy measurements [29,50,69], as well as the use of dynamic light scattering and zeta-potential [70–72], being essential to give us insight into how the interaction occurs. Regarding PaDBS1R1, clearly the lipid composition of the membrane tested is important for the initial electrostatic interactions. A preference for the Gram-negative bacteria-mimicking lipid vesicles tested (POPC:POPG 70:30, POPC:POPG:CL 65:30:05 and POPE:POPG:CL 65:30:05) was detected on the membrane dipole (Fig. 2B), DLS (Fig. 2C) and zeta-potential (Fig. 2D) results, as well as on the calculated values of K_D^{app} calculated (Table 2). The proportion between the zwitterionic (POPC and POPE) and the negatively charged phospholipids (POPG and CL) is what determines the efficiency of the interaction. Although PC lipids are generally abundant on both sides of the plasma membrane, PE lipids are mainly found on the cytoplasmic
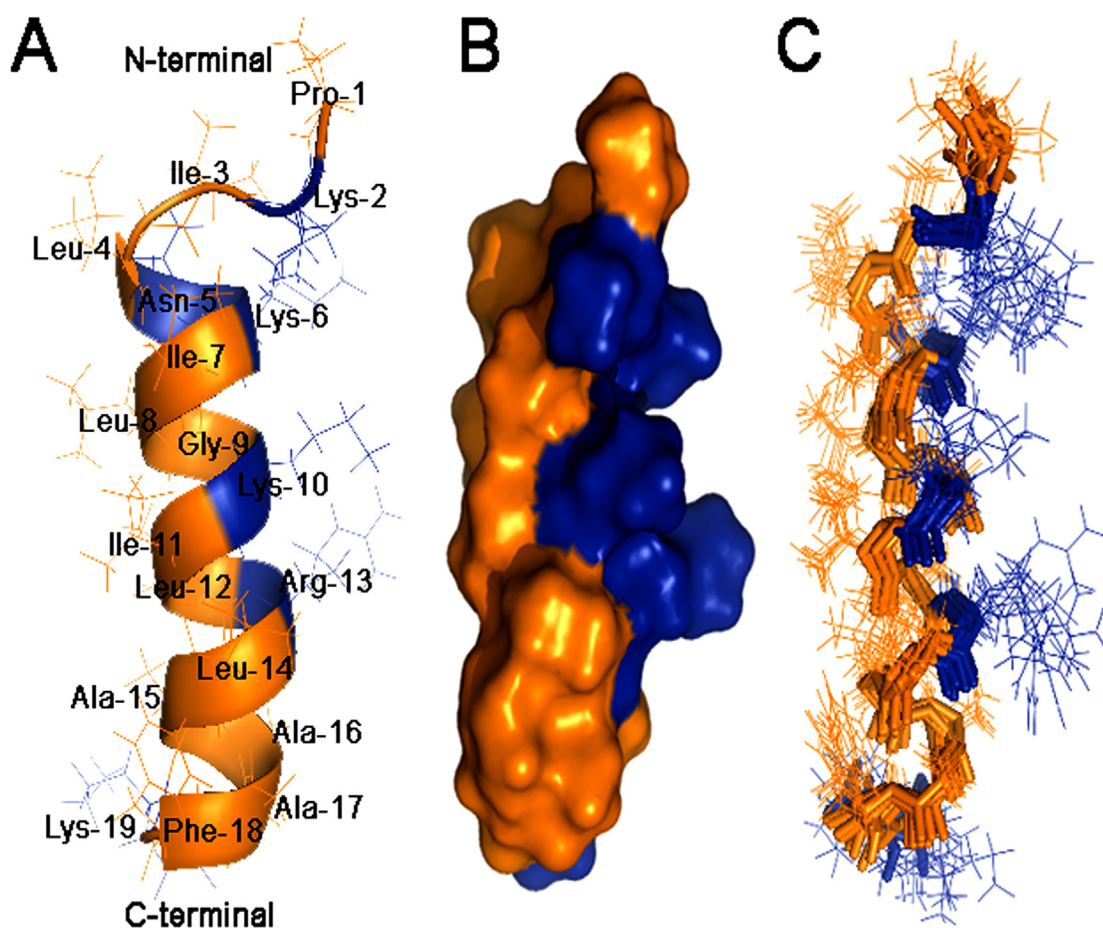
Fig. 5. NMR structure of PaDBS1R1 in SDS micelles and simulation in DOPC bilayer. (A) Hydrophilic residues are highlighted in blue and hydrophobic in orange. (B) Surface of the peptide. (C) Backbone superposition of the final 10 lower energy structures.

side of the membranes [73]. It is important to refer that for POPE containing vesicles, membrane dipole data did not show any significant variation, probably due to the fact that PaDBS1R1 induces vesicle aggregation after interaction (Fig. 2C). It can also be seen on the zeta-potential data that the peptide has a strong interaction with POPC vesicles, stronger than the interaction with membranes mimicking Gram-positive bacteria (POPC:POPG:CL and POPE:POPG:CL 25:70:05) and mammalian cells (POPC:Chol 70:30) mimicking vesicles. Even so, in the studies using di-8-ANEPPS, the interaction is one of the weakest, as expressed by its low $K_D{}^{app}$ value (Table 2). It is important to refer that, despite the lower value of apparent affinity constant, which could induce a false interpretation of stronger affinity compared to the other vesicles tested, R_{min} is also the lowest (Table 2), indicating a low amplitude of signal variation. This value is important to understand the extension of the peptide-membrane interaction. Thus, it is possible to conclude that the results are in agreement with the zeta-potential studies. Nonetheless, it is possible to infer that POPC seems to participate on the initial attraction of the peptide to the membrane, even being zwitterionic, or that PaDBS1R1 inserts on its maximum extension at very low concentrations without promoting significant membrane disturbance. Additionally, POPG plays an important role in this, which can be explained by the difference between POPC:POPG 70:30 and POPC:POPG 70:30 vesicles. PaDBS1R1 did not show any interaction with the latter ones in any of the studies done, while demonstrating preference for POPC:POPG 70:30, confirming once more that negatively charged phospholipids in the right proportion are essential for the peptide-membrane interaction. Nevertheless, beside charge, spatial arrangement in the biomembrane organization can also be important. The difference was studied by having the lipid vesicles proportionally

similar in terms of charge, but different in terms of individual components, changing POPC for POPE (65%). Directly comparing both, it was clear in all studies that PaDBS1R1 has preference for POPE containing lipid vesicles, which are more similar to the membranes found in bacteria and also documented as being more ordered, which can play an important role in peptide insertion [74]. Results obtained for POPC:-POPG:CL and POPE:POPG:CL 25:70:05 showed a lower interaction and membrane destabilization by the peptide, compared to the other anionic vesicles. This is explained by the high proportion of negatively charged lipids, 75% in these vesicles, while the vesicles with the higher affinity results present 30–35%. Even for peptides that are highly dependent of the electrostatic interactions with membranes, an increase in the anionic lipid proportion does not imply a higher affinity, contributing for a destabilization of the interaction due to the high charge density [34]. Previous reports have already described an identical behavior, suggesting a proportion of anionic lipids optimal for cationic peptide-membrane interactions consistent with our observation that POPC:POPG 70:30, POPC:POPG:CL 60:35:05 and POPE:POPG:CL 65:30:05 vesicles are those leading to higher affinity results [75].

Dynamic light scattering studies enable the detection of changes on the size of the lipid vesicles or their aggregation induced by the peptide, assessed in terms of hydrodynamic diameter (D_H). In the case of PaDBS1R1, increasing peptide concentrations only induced changes on the vesicles containing POPE, which implies that the size of the other lipid vesicles is kept constant, and that there is no significant peptide-induced membrane aggregation (Fig. 2C). The same result was also observed on the generalized polarization studies (Fig. 2A) and dynamic light scattering data (Fig. 2C), which lead us to conclude that the lipid packing distribution and the size of the lipid vesicles do not suffer any

changes when the peptide is present at the membrane interface. For POPE:POPG:CL 65:30:05 and 25:70:05, both methodologies showed that in the first PaDBS1R1 induces vesicle aggregation (Fig. 2C), with an increase of lipid packing profile (Fig. 2A). Once more, spatial arrangement and adequate negative charge proportion showed to be vital for PaDBS1R1 interaction [34]. Another possibility is that the AMP, through charge neutralization, promotes vesicle fusion by reducing charge repulsion. Reports of AMPs that promote a fusion profile can also be found in the literature, such as rBPI21 [34] and IDR-1018 [76]. For Gram-positive lipid vesicles, D_H had a small increase, mostly due to peptide accumulation near the membrane surface with the increase in concentration. Even so, this increment occurs without membrane destabilization, as shown by the other performed measurements, where the peptide does not have a preference for interaction. These results corroborate what was obtained in the antimicrobial and cytotoxicity studies, showing the preference for Gram-negative-like membranes, compared to Gram-positive bacteria or human cells.

Both the fast killing efficiency and the membrane-disruption studies indicate that the first target of the antimicrobial activity of PaDBS1R1 is the bacterial membrane, but they do not exclude the possibility of other targets essential for its activity. Lately, the number of studied AMPs that have shown activity towards intracellular components, leading to different responses, has increased, corroborating this possibility [5,76]. Understanding the interaction between AMPs and membranes is a key aspect to elucidate their mechanisms of action, at least, during the initial steps. Thus, further research is needed to determine the conformation of the peptide when interacting with lipid membranes. CD experiments showed greater structuring of PaDBS1R1 in anionic media (SDS 100% and POPC:POPG 26%) when compared to zwitterionic micelles (DPC 52%), indicating that in the first case the secondary structure of PaDBS1R1 was more defined. This can be explained by the fact that the peptide contains five positively charged amino acid residues, which favours a stronger interaction with the negatively charged SDS micelles containing sulfonate groups [77]. DPC micelles, being a zwitterionic surfactant, cannot foster greater structural stability by cationic interactions [78]. These results explain the higher activity of PaDBS1R1 against Gram-negative bacteria, like *A. baumannii*, *P. aeruginosa*, and *K. pneumoniae*.

Based on the CD spectra and NMR experiments, we propose that PaDBS1R1 adopts an amphipathic α-helical conformation in a membrane-mimetic environment (Figs. 4 and 5). This structure is probably facilitating the PaDBS1R1 insertion into the membrane by the interaction of its hydrophobic face with the membrane hydrophobic core, which could cause membrane permeabilization and further leakage of intracellular content [4,10]. Therefore, binding to the membrane is probably driven by hydrophobic and electrostatic interactions.

Widespread in nature, peptides that fold into an amphipathic α-helical conformation when interacting with their target represent successful host defense peptides [12,79]. It has been proposed that AMPs adopting such a conformation exert their killing action through mechanisms including peptide-lipid interaction followed by membrane permeation [79,80]. Consistent with this assumption, in the case of PaDBS1R1, we believe that the amphipathic α-helix conformation promotes both the electrostatic and hydrophobic interaction with the membrane, where the positive face targets the anionic bacterial surface (phospholipid polar heads) and the hydrophobic residues interact with the hydrophobic core of the membrane (phospholipid tails). Consequently, PaDBS1R1 inserts into the lipid bilayer, induces membrane disturbances including membrane permeabilization, which subsequently lead to cell lysis.

In conclusion, we demonstrated that the novel cationic antimicrobial peptide PaDBS1R1 exhibits a potent antimicrobial activity against bacteria and fungi, including antibiotic-resistant strains (*K. pneumoniae* and *S. aureus*), without cytotoxicity towards HEK-293 cells. Based on our structural and functional analysis, we have useful information on the initial interactions of PaDBS1R1 with the target membrane and its bactericidal effect. The data revealed a change in conformation upon membrane interaction, indicating that unstructured PaDBS1R1 in an aqueous environment folds into an amphipathic α-helix in the anionic membrane-mimetic environment. Our observations strongly suggest that the amphipathic α-helical PaDBS1R1 binds to the membrane through electrostatic and hydrophobic interactions that could induce membrane disturbances subsequently leading to cell death. Our findings suggest that the engineered antimicrobial peptide PaDBS1R1 is a promising candidate for the development into a therapeutic antimicrobial agent.

Supplementary data to this article can be found online at https://doi.org/10.1016/j.bbamem.2018.08.001.

Transparency document

The Transparency document associated with this article can be found, in the online version.

Acknowledgments

Conflict of interests

The authors declare that they have no conflicts of interest with the contents of this article.

Author contributions

OLF and AL designed research and coordinated the project; LNI, WFP, IMF, COM, MRF, SMR, VH performed experiments and analysed data with ESFA, NCS, SG, LML, AL and OLF; LNI, WFP, ESFA and MRF wrote the article; ESFA, COM and LML were responsible for structural propose by NMR and CD.

References

[1] A.R. Coates, G. Halls, Y. Hu, Novel classes of antibiotics or more of the same? Br. J. Pharmacol. 163 (2011) 184–194, https://doi.org/10.1111/j.1476-5381.2011.01250.x.

[2] F.H. Waghu, L. Gopi, R.S. Barai, P. Ramteke, B. Nizami, S. Idicula-Thomas, CAMP: collection of sequences and structures of antimicrobial peptides, Nucleic Acids Res. 42 (2014) D1154–D1158, https://doi.org/10.1093/nar/gkt1157.

[3] M. Pasupuleti, A. Schmidtchen, M. Malmsten, Antimicrobial peptides: key components of the innate immune system, Crit. Rev. Biotechnol. 32 (2012) 143–171, https://doi.org/10.3109/07388551.2011.594423.

[4] K.A. Brogden, Antimicrobial peptides: pore formers or metabolic inhibitors in bacteria? Nat. Rev. Microbiol. 3 (2005) 238–250, https://doi.org/10.1038/nrmicro1098.

[5] R.E. Hancock, Cationic peptides: effectors in innate immunity and novel antimicrobials, Lancet Infect. Dis. 1 (2001) 156–164, https://doi.org/10.1016/S1473-3099(01)00092-5.

[6] J.G. Hurdle, A.J. O'Neill, I. Chopra, R.E. Lee, Targeting bacterial membrane function: an underexploited mechanism for treating persistent infections, Nat. Rev. Microbiol. 9 (2011) 62–75, https://doi.org/10.1038/nrmicro2474.

[7] M.R. Yeaman, N.Y. Yount, Mechanisms of antimicrobial peptide action and resistance, Pharmacol. Rev. 55 (2003) 27–55, https://doi.org/10.1124/pr.55.1.2.

[8] L.T. Nguyen, E.F. Haney, H.J. Vogel, The expanding scope of antimicrobial peptide structures and their modes of action, Trends Biotechnol. 29 (2011) 464–472, https://doi.org/10.1016/j.tibtech.2011.05.001.

[9] W.C. Wimley, K. Hristova, Antimicrobial peptides: successes, challenges and unanswered questions, J. Membr. Biol. 239 (2011) 27–34, https://doi.org/10.1007/s00232-011-9343-0.

[10] R.F. Epand, L. Maloy, A. Ramamoorthy, R.M. Epand, Amphipathic helical cationic antimicrobial peptides promote rapid formation of crystalline states in the presence of phosphatidylglycerol: lipid clustering in anionic membranes, Biophys. J. 98 (2010) 2564–2573, https://doi.org/10.1016/j.bpj.2010.03.002.

[11] M.A. Sani, F. Separovic, How membrane-active peptides get into lipid membranes, Acc. Chem. Res. 49 (2016) 1130–1138, https://doi.org/10.1021/acs.accounts.6b00074.

[12] A. Giangaspero, L. Sandri, A. Tossi, Amphipathic alpha helical antimicrobial peptides, Eur. J. Biochem. 268 (2001) 5589–5600, https://doi.org/10.1046/j.1432-1033.2001.02494.x.

[13] Y. Jin, J. Hammer, M. Pate, Y. Zhang, F. Zhu, E. Zmuda, J. Blazyk, Antimicrobial activities and structures of two linear cationic peptide families with various amphipathic beta-sheet and alpha-helical potentials, Antimicrob. Agents Chemother. 49 (2005) 4957–4964, https://doi.org/10.1128/AAC.49.12.4957-4964.2005.

[14] S. Maria-Neto, S. Candido Ede, D.R. Rodrigues, D.A. de Sousa, E.M. da Silva, L.M. de Moraes, J. Otero-Gonzalez Ade, B.S. Magalhaes, S.C. Dias, O.L. Franco, Deciphering the magainin resistance process of *Escherichia coli* strains in light of the cytosolic proteome, Antimicrob. Agents Chemother. 56 (2012) 1714–1724, https://doi.org/10.1128/AAC.05558-11.

[15] E.C. Spindler, N.R. Boyle, R.E. Hancock, R.T. Gill, Genome-wide identification of genes conferring energy related resistance to a synthetic antimicrobial peptide (Bac8c), PLoS One 8 (2013) e55052, , https://doi.org/10.1371/journal.pone.0055052.

[16] V.I. Band, D.S. Weiss, Mechanisms of antimicrobial peptide resistance in Gram-negative bacteria, Antibiotics 4 (2015) 18–41, https://doi.org/10.3390/antibiotics4010018.

[17] C.D. Fjell, H. Jenssen, W.A. Cheung, R.E. Hancock, A. Cherkasov, Optimization of antibacterial peptides by genetic algorithms and cheminformatics, Chem. Biol. Drug Des. 77 (2011) 48–56, https://doi.org/10.1111/j.1747-0285.2010.01044.x.

[18] W.F. Porto, O.N. Silva, O.L. Franco, Prediction and rational design of antimicrobial peptides, in: E. Faraggi (Ed.), Protein Struct. InTech, 2012, pp. 377–396, , https://doi.org/10.5772/2335.

[19] C. Loose, K. Jensen, I. Rigoutsos, G. Stephanopoulos, A linguistic model for the rational design of antimicrobial peptides, Nature 443 (2006) 867–869, https://doi.org/10.1038/nature05233.

[20] W.F. Porto, I.C.M. Fensterseifer, S.M. Ribeiro, O.L. Franco, Joker: an algorithm to insert patterns into sequences for designing antimicrobial peptides, Biochim. Biophys. Acta (2018), https://doi.org/10.1016/j.bbagen.2018.06.011.

[21] L.N. Irazazabal, W.F. Porto, S.M. Ribeiro, S. Casale, V. Humblot, A. Ladram, O.L. Franco, Selective amino acid substitution reduces cytotoxicity of the antimicrobial peptide mastoparan, Biochim. Biophys. Acta (2016), https://doi.org/10.1016/j.bbamem.2016.07.001.

[22] NCCLS, Methods for Dilution Antimicrobial Susceptibility Tests for Bacteria that Grow Aerobically, NCCLS Document, Vols. M7–A6 (2003) (19087–11898).

[23] T.L. Riss, R.A. Moravec, A.L. Niles, H.A. Benink, T.J. Worzella, L. Minor, D. Storts, Y. Reid, Cell viability assays, in: G.S. Sittampalam, N.P. Coussens, H. Nelson, M. Arkin, D. Auld, C. Austin (Eds.), Assay Guidance Manual, Bethesda (MD), 2004.

[24] W.F. Porto, L. Irazazabal, E.S.F. Alves, S.M. Ribeiro, C.O. Matos, A.S. Pires, I.C.M. Fensterseifer, V.J. Miranda, E.F. Haney, V. Humblot, M.D.T. Torres, R.E.W. Hancock, L.M. Liao, A. Ladram, T.K. Lu, C. de la Fuente-Nunez, O.L. Franco, In silico optimization of a guava antimicrobial peptide enables combinatorial exploration for peptide design, Nat. Commun. 9 (2018) 1490, https://doi.org/10.1038/s41467-018-03746-3.

[25] Y. Chen, C.T. Mant, S.W. Farmer, R.E. Hancock, M.L. Vasil, R.S. Hodges, Rational design of alpha-helical antimicrobial peptides with enhanced activities and specificity/therapeutic index, J. Biol. Chem. 280 (2005) 12316–12329, https://doi.org/10.1074/jbc.M413406200.

[26] L.D. Mayer, M.J. Hope, P.R. Cullis, Vesicles of variable sizes produced by a rapid extrusion procedure, Biochim. Biophys. Acta 858 (1986) 161–168.

[27] A. Lisi, D. Pozzi, S. Grimaldi, Use of the fluorescent probe Laurdan to investigate structural organization of the *vesicular stomatitis virus* (VSV) membrane, Membr. Biochem. 10 (1993) 203–212.

[28] P.L. Chong, P.T. Wong, Interactions of Laurdan with phosphatidylcholine liposomes: a high pressure FTIR study, Biochim. Biophys. Acta 1149 (1993) 260–266.

[29] S. Gonçalves, A. Teixeira, J. Abade, L.N. de Medeiros, E. Kurtenbach, N.C. Santos, Evaluation of the membrane lipid selectivity of the pea defensin Psd1, Biochim. Biophys. Acta 1818 (2012) 1420–1426, https://doi.org/10.1016/j.bbamem.2012.02.012.

[30] E. Gross, R.S. Bedlack Jr., L.M. Loew, Dual-wavelength ratiometric fluorescence measurement of the membrane dipole potential, Biophys. J. 67 (1994) 208–216, https://doi.org/10.1016/S0006-3495(94)80471-0.

[31] P.M. Matos, M.A. Castanho, N.C. Santos, HIV-1 fusion inhibitor peptides enfuvirtide and T-1249 interact with erythrocyte and lymphocyte membranes, PLoS One 5 (2010) e9830, , https://doi.org/10.1371/journal.pone.0009830.

[32] A. Hollmann, P.M. Matos, M.T. Augusto, M.A. Castanho, N.C. Santos, Conjugation of cholesterol to HIV-1 fusion inhibitor C34 increases peptide-membrane interactions potentiating its action, PLoS One 8 (2013) e60302, , https://doi.org/10.1371/journal.pone.0060302.

[33] J. Cladera, P. O'Shea, Intramembrane molecular dipoles affect the membrane insertion and folding of a model amphiphilic peptide, Biophys. J. 74 (1998) 2434–2442, https://doi.org/10.1016/S0006-3495(98)77951-2.

[34] M.M. Domingues, M.A. Castanho, N.C. Santos, rBPI(21) promotes lipopolysaccharide aggregation and exerts its antimicrobial effects by (hemi)fusion of PG-containing membranes, PLoS One 4 (2009) e8385, , https://doi.org/10.1371/journal.pone.0008385.

[35] S.W. Provencher, A constrained regularization method for inverting data represented by linear algebraic or integral equations, Comput. Phys. Commun. 27 (1982) 213–227, https://doi.org/10.1016/0010-4655(82)90173-4.

[36] S.W. Provencher, CONTIN: a general purpose constrained regularization program for inverting noisy linear algebraic and integral equations, Comput. Phys. Commun. 27 (1982) 229–242, https://doi.org/10.1016/0010-4655(82)90174-6.

[37] J.M. Freire, M.M. Domingues, J. Matos, M.N. Melo, A.S. Veiga, N.C. Santos, M.A. Castanho, Using zeta-potential measurements to quantify peptide partition to lipid membranes, Eur. Biophys. J. 40 (2011) 481–487, https://doi.org/10.1007/s00249-010-0661-4.

[38] P.M. Carvalho, M.R. Felício, N.C. Santos, S. Gonçalves, M.M. Domingues, Application of light scattering techniques to nanoparticle characterization and development, Front. Chem. 6 (2018) 237, https://doi.org/10.3389/fchem.2018.00237.

[39] K. Thevissen, F.R. Terras, W.F. Broekaert, Permeabilization of fungal membranes by plant defensins inhibits fungal growth, Appl. Environ. Microbiol. 65 (1999) 5451–5458.

[40] P.J. Sims, A.S. Waggoner, C.H. Wang, J.F. Hoffman, Studies on the mechanism by which cyanine dyes measure membrane potential in red blood cells and phosphatidylcholine vesicles, Biochemistry 13 (1974) 3315–3330.

[41] F. Abbassi, Z. Raja, B. Oury, E. Gazanion, C. Piesse, D. Sereno, P. Nicolas, T. Foulon, A. Ladram, Antibacterial and leishmanicidal activities of temporin-SHd, a 17-residue long membrane-damaging peptide, Biochimie 95 (2013) 388–399, https://doi.org/10.1016/j.biochi.2012.10.015.

[42] Y.H. Chen, J.T. Yang, K.H. Chau, Determination of the helix and beta form of proteins in aqueous solution by circular dichroism, Biochemistry 13 (1974) 3350–3359.

[43] K. Wüthrich, NMR of Proteins and Nucleic Acids, New York (1986).

[44] F. Delaglio, S. Grzesiek, G.W. Vuister, G. Zhu, J. Pfeifer, A. Bax, NMRPipe: a multidimensional spectral processing system based on UNIX pipes, J. Biomol. NMR 6 (1995) 277–293.

[45] B.A. Johnson, R.A. Blevins, NMR view: a computer program for the visualization and analysis of NMR data, J. Biomol. NMR 4 (1994) 603–614, https://doi.org/10.1007/BF00404272.

[46] C.D. Schwieters, J.J. Kuszewski, N. Tjandra, G.M. Clore, The Xplor-NIH NMR molecular structure determination package, J. Magn. Reson. 160 (2003) 65–73.

[47] C. Schwieters, J. Kuszewski, G. Marius Clore, Using Xplor–NIH for NMR molecular structure determination, Prog. Nucl. Magn. Reson. Spectrosc. 48 (1) (2006) 47–62.

[48] P.Y. Muller, M.N. Milton, The determination and interpretation of the therapeutic index in drug development, Nat. Rev. Drug Discov. 11 (2012) 751–761, https://doi.org/10.1038/nrd3801.

[49] S. Rex, Pore formation induced by the peptide melittin in different lipid vesicle membranes, Biophys. Chem. 58 (1996) 75–85.

[50] P.M. Matos, H.G. Franquelim, M.A. Castanho, N.C. Santos, Quantitative assessment of peptide-lipid interactions. Ubiquitous fluorescence methodologies, Biochim. Biophys. Acta 1798 (2010) 1999–2012, https://doi.org/10.1016/j.bbamem.2010.07.012.

[51] M.M. Domingues, P.S. Santiago, M.A. Castanho, N.C. Santos, What can light scattering spectroscopy do for membrane-active peptide studies? J. Pept. Sci. 14 (2008) 394–400, https://doi.org/10.1002/psc.1007.

[52] K. Wuthrich, Sequential individual resonance assignments in the 1H-NMR spectra of polypeptides and proteins, Biopolymers 22 (1983) 131–138, https://doi.org/10.1002/bip.360220121.

[53] D.S. Wishart, B.D. Sykes, F.M. Richards, The chemical shift index: a fast and simple method for the assignment of protein secondary structure through NMR spectroscopy, Biochemistry 31 (1992) 1647–1651.

[54] Y. Shen, F. Delaglio, G. Cornilescu, A. Bax, TALOS +: a hybrid method for predicting protein backbone torsion angles from NMR chemical shifts, J. Biomol. NMR 44 (2009) 213–223, https://doi.org/10.1007/s10858-009-9333-z.

[55] S.B. Nabuurs, C.A. Spronk, E. Krieger, H. Maassen, G. Vriend, G.W. Vuister, Quantitative evaluation of experimental NMR restraints, J. Am. Chem. Soc. 125 (2003) 12026–12034, https://doi.org/10.1021/ja035440f.

[56] J.P. Linge, M.A. Williams, C.A. Spronk, A.M. Bonvin, M. Nilges, Refinement of

protein structures in explicit solvent, Proteins 50 (2003) 496–506, https://doi.org/10.1002/prot.10299.

[57] S.B. Nabuurs, C.A.E.M. Spronk, G. Vriend, G.W. Vuister, Concepts and tools for NMR restraint analysis and validation, Concepts Magn. Reson. 22A (2004) 90–105.

[58] R. Koradi, M. Billeter, K. Wuthrich, MOLMOL: a program for display and analysis of macromolecular structures, J. Mol. Graph. 14 (1996) 51–55 (29–32).

[59] C.A. Spronk, S.B. Nabuurs, A.M. Bonvin, E. Krieger, G.W. Vuister, G. Vriend, The precision of NMR structure ensembles revisited, J. Biomol. NMR 25 (2003) 225–234.

[60] G.N. Ramachandran, C. Ramakrishnan, V. Sasisekharan, Stereochemistry of poly-peptide chain configurations, J. Mol. Biol. 7 (1963) 95–99.

[61] C. Ramakrishnan, G.N. Ramachandran, Stereochemical criteria for polypeptide and protein chain conformations. II. Allowed conformations for a pair of peptide units, Biophys. J. 5 (1965) 909–933, https://doi.org/10.1016/S0006-3495(65)86759-5.

[62] H. Katayama, T. Ohira, K. Aida, H. Nagasawa, Significance of a carboxyl-terminal amide moiety in the folding and biological activity of crustacean hyperglycemic hormone, Peptides 23 (2002) 1537–1546.

[63] M.F. Ali, A. Soto, F.C. Knoop, J.M. Conlon, Antimicrobial peptides isolated from skin secretions of the diploid frog, *Xenopus tropicalis* (Pipidae), Biochim. Biophys. Acta 1550 (2001) 81–89.

[64] N. Papo, Y. Shai, Can we predict biological activity of antimicrobial peptides from their interactions with model phospholipid membranes? Peptides 24 (2003) 1693–1703, https://doi.org/10.1016/j.peptides.2003.09.013.

[65] O.N. Silva, K.C. Mulder, A.E. Barbosa, A.J. Otero-Gonzalez, C. Lopez-Abarrategui, T.M. Rezende, S.C. Dias, O.L. Franco, Exploring the pharmacological potential of promiscuous host-defense peptides: from natural screenings to biotechnological applications, Front. Microbiol. 2 (2011) 232, https://doi.org/10.3389/fmicb.2011.00232.

[66] Y. Shai, Mode of action of membrane active antimicrobial peptides, Biopolymers 66 (2002) 236–248, https://doi.org/10.1002/bip.10260.

[67] J.M. Freire, D. Gaspar, B.G. de la Torre, A.S. Veiga, D. Andreu, M.A. Castanho, Monitoring antibacterial permeabilization in real time using time-resolved flow cytometry, Biochim. Biophys. Acta 1848 (2015) 554–560, https://doi.org/10.1016/j.bbamem.2014.11.001.

[68] M.R. Felício, O.N. Silva, S. Gonçalves, N.C. Santos, O.L. Franco, Peptides with dual antimicrobial and anticancer activities, Front. Chem. 5 (2017) 5, https://doi.org/10.3389/fchem.2017.00005.

[69] S. Gonçalves, P.M. Silva, M.R. Felício, L.N. de Medeiros, E. Kurtenbach, N.C. Santos, Psd1 effects on *Candida albicans* planktonic cells and biofilms, Front. Cell. Infect. Microbiol. 7 (2017) 249, https://doi.org/10.3389/fcimb.2017.00249.

[70] C.S. Alves, M.N. Melo, H.G. Franquelim, R. Ferre, M. Planas, L. Feliu, E. Bardaji, W. Kowalczyk, D. Andreu, N.C. Santos, M.X. Fernandes, M.A. Castanho, Escherichia coli cell surface perturbation and disruption induced by antimicrobial peptides BP100 and pepR, J. Biol. Chem. 285 (2010) 27536–27544, https://doi.org/10.1074/jbc.M110.130955.

[71] M.C. Manzini, K.R. Perez, K.A. Riske, J.C. Bozelli Jr., T.L. Santos, M.A. da Silva, G.K. Saraiva, M.J. Politi, A.P. Valente, F.C. Almeida, H. Chaimovich, M.A. Rodrigues, M.P. Bemquerer, S. Schreier, I.M. Cuccovia, Peptide:lipid ratio and membrane surface charge determine the mechanism of action of the antimicrobial peptide BP100. Conformational and functional studies, Biochim. Biophys. Acta 1838 (2014) 1985–1999, https://doi.org/10.1016/j.bbamem.2014.04.004.

[72] M.M. Domingues, P.M. Silva, H.G. Franquelim, F.A. Carvalho, M.A. Castanho, N.C. Santos, Antimicrobial protein rBPI21-induced surface changes on Gram-ne-gative and Gram-positive bacteria, Nanomedicine 10 (2014) 543–551, https://doi.org/10.1016/j.nano.2013.11.002.

[73] B. Fadeel, D. Xue, The ins and outs of phospholipid asymmetry in the plasma membrane: roles in health and disease, Crit. Rev. Biochem. Mol. Biol. 44 (2009) 264–277, https://doi.org/10.1080/10409230903193307.

[74] F. Separovic, K. Gawrisch, Effect of unsaturation on the chain order of phosphati-dylcholines in a dioleoylphosphatidylethanolamine matrix, Biophys. J. 71 (1996) 274–282, https://doi.org/10.1016/S0006-3495(96)79223-8.

[75] M.M. Ribeiro, M.M. Domingues, J.M. Freire, N.C. Santos, M.A. Castanho, Translocating the blood-brain barrier using electrostatics, Front. Cell. Neurosci. 6 (2012) 44, https://doi.org/10.3389/fncel.2012.00044.

[76] S.C. Mansour, C. de la Fuente-Nunez, R.E. Hancock, Peptide IDR-1018: modulating the immune system and targeting bacterial biofilms to treat antibiotic-resistant bacterial infections, J. Pept. Sci. 21 (2015) 323–329, https://doi.org/10.1002/psc.2708.

[77] J. Oremusova, A. Lengyel, Critical Micelle Concentration of Ionic Surfactants, (2007).

[78] H. Khandelia, Y.N. Kaznessis, Molecular dynamics investigation of the influence of anionic and zwitterionic interfaces on antimicrobial peptides' structure: implica-tions for peptide toxicity and activity, Peptides 27 (2006) 1192–1200, https://doi.org/10.1016/j.peptides.2005.10.022.

[79] M. Dathe, T. Wieprecht, Structural features of helical antimicrobial peptides: their potential to modulate activity on model membranes and biological cells, Biochim. Biophys. Acta 1462 (1999) 71–87.

[80] Z. Oren, Y. Shai, Mode of action of linear amphipathic alpha-helical antimicrobial peptides, Biopolymers 47 (1998) 451–463, https://doi.org/10.1002/(SICI)1097-0282(1998)47:6<451::AID-BIP4>3.0.CO;2-F.